13

Laser-stimulated metal-induced crystallization of silicon coatings on film and nanofiber polymer substrates

© A.A. Serdobintsev, A.M. Kartashova, P.A. Demina, L.D. Volkovoynova, I.O. Kozhevnikov, V.V. Galushka

Saratov National Research State University,
410012 Saratov, Russia
e-mail: loris.volkoff@gmail.com

Received January 16, 2023
Revised January 16, 2023
Accepted January 16, 2023.

The development of basic technological approaches to the creation of flexible electronic devices is an actual problem nowadays. This paper presents the results of forming nanocrystalline silicon coatings on various kinds of flexible polymer substrates. The coatings were obtained by laser-stimulated metal-induced crystallization. Fully crystallized silicon films on an area of $30 \times 30\,\mu$m on a polyimide film substrate using this technique were obtained. The applicability of this technique to the silicon coating on a nanofiber polymer substrate obtained by electrospinning is demonstrated. The range of laser fluence value which leads to the crystallization of silicon with minimal damage to nanofiber substrates has been determined. The degree of damage to the substrates was assessed using scanning electron microscopy. The results of experimental studies confirming the formation of crystallized silicon coatings on nanofiber polymer substrates are presented.

Keywords: flexible electronics, metal-induced silicon crystallization, laser-induced silicon crystallization, infrared laser, nanofiber nonwovens.

DOI: 10.21883/0000000000

Introduction

Currently , semiconductor nano- and submicron materials, for example, thin films, are used in many areas of human activity, which influences the growing number of studies of their properties and ways to improve functionality [1–3]. The areas of application of semiconductor nano- and submicron materials are very wide, for example, they are used in micro- and nanoelectronics [4], solar energy [5], sensorics [6]. For the most part, these materials are amorphous in their original form. And, although their amorphous form is also widely used in various fields [7], the use of semiconductor materials in the crystalline state often makes it possible to create more efficient devices, sensors and converters [8]. In connection with this, there is a need for methods which allow to obtain crystallized semiconductor materials. There are many ways to transform amorphous materials into crystalline ones, but almost all of them involve a fairly intense thermal effect on the crystallized material. This circumstance significantly narrows the range of materials that can be used as substrates for applying silicon coatings. In particular, polymer materials are almost completely excluded due to low temperature resistance, which, in turn, significantly complicates the creation of flexible sensor systems and solar cells based on polycrystalline silicon coatings.

Currently , there is great interest in the development of new methods for forming poly-Si films on low-melting substrates [9]. The application of polymer substrates allows to create flexible electronic devices based on silicon, which will expand the scope of application of these devices. Silicon is often crystallized using excimer [10] and femtosecond lasers [11]. To simplify and reduce the cost of the crystallization process, an original method of metal-induced laser-stimulated (MILS) crystallization of amorphous silicon on low-melting substrates [12] was developed, which is also applicable to silicon coatings deposited on polymer films [13]. The key point of the MILS process is the crystallization of an amorphous silicon coating with a pulsed infrared laser using a metal absorbing layer. The application of certain metals (aluminum, tin, gold [14]) makes it possible to reduce the crystallization temperature of silicon due to the formation of the eutectic phase. The polymer substrate is transparent to infrared radiation, like the silicon coating, which allows to virtually eliminate its heating and degradation during laser processing.

In this work, the substrates are polyimide (PI) film and nonwoven nanofibrous material obtained by electrospinning from a polyacrylonitrile (PAN) solution.

1. Methods of creation and investigation of samples

Nonwoven substrates were obtained by electrospinning from a solution of polyacrylonitrile (PAN, $(C_3H_3N)_n$ in dimethylformamide (DMF, C_3H_7NO). Electroforming was carried out using a syringe pump „SPLab02“ and a high-voltage power supply FUG HCP 140−65000. For the initial PAN solution, 0.661 g dry matter and 5.046 ml DMFA were used. Mixing until homogeneity was carried out using a heated magnetic stirrer. The temperature was set to 323 K,

and the time spent on dissolution was 3 h. The first hour the mixing intensity was 350 rpm, the second — 500 rpm, the third — 650 rpm. After 2 h mixing, another 1 ml DMFA was added. After complete dissolution of the dry substance, the solution was poured into a syringe, which was fixed to the unit. The distance from the end of the needle to the collector with the substrate was set equal to 25 cm. Colored thick paper was used as a substrate. The rate of squeezing the solution out of the syringe was set to 1 ml/h. The process lasted 15 min, while the voltage at the source was equal to $U = 53$ kV. The needle was grounded during the electrospinning process, and a negative potential was applied to the collector.

The samples were created by sequential sputtering of silicon and then aluminum onto polymer substrates (film PI and nanofibrous PAN). Sputtering was carried out in a Nexdep magnetron sputtering unit (Angstrom, Canada) in an argon environment. The residual pressure was $2.6 \cdot 10^{-3}$ Pa, the working pressure after argon injection was $4.5 \cdot 10^{-1}$ Pa. Two magnetron sources are mounted in the vacuum chamber of the unit under disk targets with a diameter of 76.2 mm, which allows sputtering of both layers without devacuuming the chamber. We used targets made of silicon with a purity of 99.999% and aluminum with a purity of 99.9% produced by LLC „Girmet" (Russia). The thickness of both targets was 6 mm. The substrates were fixed using a shadow mask with six holes in the form of squares with dimensions 12×12 mm. The mask is required to prevent bending of the polyimide, which can lead to uneven coverage and distortion during laser processing. Thus, in one sputtering cycle, six identical two-layer samples in the shape of 12×12 mm squares were obtained on a polyimide substrate.

During the sputtering process, the power of the magnetron sources was maintained at a constant level. For silicon it is 500 W, for aluminum — 300 W. The thickness of the sprayed layers was controlled using piezoquartz sensors installed in a vacuum chamber and a sputtering rate control system (Sycon, USA). For samples on PI, the thickness of the aluminum layer was 100 nm, the thickness of the silicon layer was — 900 nm. In the case of using electrospun PAN substrates, the thickness of the layers was reduced to 150 nm (Si) and 30 nm (Al) for the following reason: it is preferable that the thickness of the silicon coating does not exceed its width, determined by the fiber diameter. Taking into account the fact that the average diameter of the nonwoven material fibers was approximately 500 nm, it seems advisable to work with silicon layers approximately 3 times thinner. The thickness of the aluminum layer was also reduced in an appropriate manner. The thickness of the PI substrate was 500 μm, the thickness of the PAN substrate was 200 μm. No additional heating of the substrate was used during the sputtering process.

Laser processing of the samples was carried out using a MiniMarker 2 unit (Laser Center, Russia), equipped with a pulsed fiber laser with a wavelength of 1064 nm (YAG:Nd) and an optical scanner. Annealing was carried out from the aluminum film side. On each film sample, a square area of size 10×10 mm was processed in the scanning mode at a fixed fluence value, which varied in the range from 8.42 to 28 J/cm ^{2} from sample to sample. For samples on nonwoven PAN, 2×2 mm squares were also processed in scanning mode; the fluence varied in the range from 0.279 to 0.457 J/cm^2; at high fluences, there was melting of the nonwoven substrate. The fluence changed in both cases by changing the speed of the laser beam, since changing the speed changes the number of pulses per point on the sample surface, as well as the area of their overlap. This is due to the fact that processing speed is critical in industrial production, so this particular characteristic was chosen as variable. Other parameters of laser processing were constant: radiation power 0.2 W, pulse frequency 99 kHz, pulse width is 100 ns.

The structure of the samples was studied by Raman scattering spectroscopy (RSS) using InVia microscope (Renishaw, UK). A laser with a wavelength of 532 nm was used for the study. The signal accumulation time was 10 s at each point at a radiation power of 0.125 mW, the laser spot size was 1.3 μm. Such parameters of probing radiation make it possible, on the one hand, to avoid crystallization of amorphous silicon directly during the measurement process, and on the other hand, they make it possible to obtain results with a high „signal-to-noise " ratio.

Measurements were carried out at 900 points on each sample (matrix 30×30 points) on the PI film, the distance between adjacent points was 1 μm. The resulting spectra were then averaged for each sample to minimize errors.

For samples on nonwoven PAN, the number of measured points was significantly less due to the fibrous structure of the sample. At each laser-annealed area, RS spectra were recorded at 4 points, after which the results were also averaged.

Scanning electron microscopy (SEM) was carried out using a Tescan Mira II microscope (Czech Republic).

2. Results and discussion

2.1. Samples on polyimide film

When a two-layer aluminum-silicon structure deposited on a flexible polymer substrate is irradiated, infrared laser radiation is actually absorbed only by the aluminum layer. The energy absorbed by aluminum is partially spent on ablation of the aluminum layer, and the remaining part is transferred to the underlying silicon layer through heat transfer [15]. This part of the energy transferred to the silicon layer promotes its crystallization.

Figure 1 shows the RS spectra averaged over nine hundred measured points for the studied samples on PI film. RS spectra were recorded from the silicon film side. The spectrum of the initial amorphous silicon film, recorded in the above mode immediately after sputtering, was obtained from an additionally sputtered sample with one layer of amorphous silicon 900 nm thick, since the

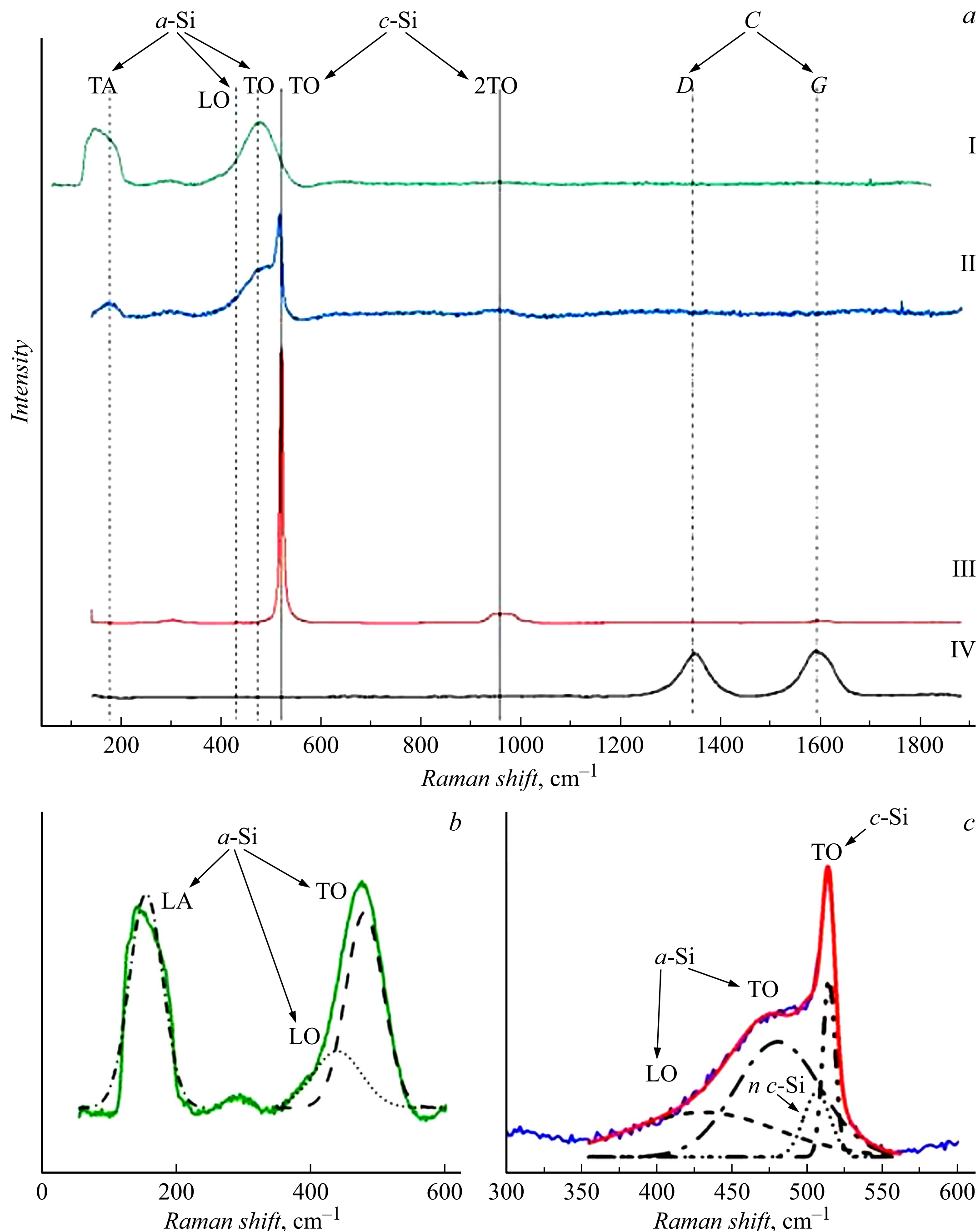

Figure 1. Averaged RS spectra for the studied samples on polyimide substrates: *a* –I — initial amorphous silicon film (the intensity value is increased by 10 times), II — laser treatment with a fluence of 8.42 J/cm^2 (the intensity value is increased by 20 times), III — 18.2 J/cm^2, IV — 28 J/cm^2; *b* — area 50–600 cm^{-1} graphics I with decomposition into components; *c* — area 400–600 cm^{-1} graphics II with decomposition into components.

aluminum layer shields the silicon layer from the probing laser beam during RS recording. It should be noted that for laser-processed samples, shielding does not occur, since during the processing the aluminum layer is predominantly ablated [12,13].

The spectrum clearly distinguishes the TA (154 cm^{-1}) and LO + TO (433 and 477 cm^{-1}) modes characteristic of the amorphous silicon phase. No peaks of the crystalline phase are observed, thus, immediately after sputtering, the silicon layer was completely amorphous.

At a fluence of 8.42 J/cm^2, a peak appears in the spectrum in the region of 514 cm^{-1}, corresponding to the TO mode of the crystalline phase of silicon. The integrated intensity of the TO mode peak of the amorphous phase is comparable to the integral intensity of the TO mode of the crystalline phase, which indicates a significant proportion of

the amorphous component in the silicon coating. Thus, we can conclude that the fluence is insufficient for complete crystallization of silicon.

As the laser processing fluence in the RS spectra increases, the intensity of the TO mode of the crystalline phase of silicon increases, and the intensity of the amorphous modes decreases. At a fluence of 18.2 J/cm^2, the resulting spectrum shows the presence of only the crystalline phase of silicon; it is not possible to identify the peaks corresponding to the amorphous component, despite averaging over nine hundred points (graph *c* in Fig. 1). The peak of the TO mode of crystalline silicon, located in the region of 518 cm^{-1}, is almost symmetrical, and its width at half maximum (half-width) is comparable to the half-width of a single-crystalline silicon sample (7.7 and 3.9 cm^{-1}, respectively), which indicates good quality of the crystalline structure in the sample [17]. The shift of the peak positions relative to the tabulated value for single crystalline silicon is due to the small sizes of crystallites, which will be discussed in detail below. It should be mentioned that there are no polyimide peaks (the most intense for the substrate used are located in the region of 1786 and 1392 cm^{-1}) in the RS spectrum of this sample, therefore, the resulting film of crystallized silicon is continuous.

A further increase in fluence ultimately leads to the destruction of the silicon coating. Thus, the spectrum of a sample processed at a fluence of 28 J/cm^2 does not contain peaks corresponding to the amorphous or crystalline phases of silicon. It should be noted that during laser processing with such a high fluence, there is a black coating on the surface of the sample. From an analysis of the literature data, we can conclude that the RS spectrum of this coating contains only characteristic peaks corresponding to carbon (D-mode at 1346 cm^{-1} and G-mode at 1594 cm^{-1}) [18]. Most likely, at such a high fluence, complete ablation of not only the aluminum layer, but also the silicon layer occurred. In this case, the near-surface layer of the polyimide substrate underwent carbonization [19], which is confirmed by RS measurements. The above considerations allow to come to the conclusion that this fluence value is clearly redundant for the crystallization of an amorphous silicon layer with a thickness of 1 μm on a PI substrate.

Based on the averaged RS spectra, the volume fraction of the crystalline phase of silicon was calculated using formulas (1) and (2) in accordance with the work [20]:

$$\rho_c = I_c/(I_c + yI_a), \tag{1}$$

where I_c — peak intensity of crystalline silicon, I_a — peak intensity of amorphous silicon, y — ratio of integral Raman scattering cross sections for crystalline and bulk phases.

$$y(L) = 1 + L/50 \cdot \exp(-L/250), \tag{2}$$

where L — crystallite size, expressed in angstroms.

The crystallite size to determine the ratio of scattering cross sections in the amorphous and crystalline phases was calculated in accordance with the work [21]:

$$L = \alpha(-A/\Delta\omega)^{1/\gamma}, \tag{3}$$

where α — lattice constant of silicon, it is equal to 0.543 nm, γ and A describe vibrations in a nanocrystal taking into account the size limitation, $\Delta\omega$ — the Raman shift of the position of the peak of a nanocrystal relative to the value of the position of the peak of single crystal silicon.

The calculated values of the average crystallite size and the fraction of the crystalline phase in the studied samples are presented in Table 1.

Table 1. Average crystallite size and fraction of the crystalline phase in samples on PI substrates processed at different fluences

Fluence, J/cm^2	Share crystallized	Size crystallite, nm	Size silicon crystallite acc. [22], nm
18.2	1	4.6	6.0
10.2	0.34	4.3	5.9
8.42	0.15	2.3	2.8

For comparison, the values of crystallite sizes determined from the results of calculations from the work [22] are given. The crystallite sizes determined using two different methods are quite close, but calculation using formula (3) gives slightly smaller values. The observed discrepancy in sizes may be due to the constants γ and A, the values of which were taken from the work [21] without any correction. Nevertheless, both approaches allow to estimate the average crystallite size in samples and identify a tendency for its increase with increasing laser processing fluence.

The measurement results show that with increasing fluence, the volume fraction of crystallized silicon increases, as well as the size of the crystallites. The fluence of 18.2 J/cm^2 should be considered optimal for the given thickness ratio of the silicon and aluminum layers (9:1). As mentioned above, it is not possible to isolate peaks corresponding to the modes of the amorphous component from the average spectrum of the corresponding sample; therefore, calculation using formula (1) gives a fraction of the crystalline component equal to unity. Moreover, all the resulting coatings are nanocrystalline; even for a completely crystallized sample, the average crystallite size does not exceed 4.6 nm. Analysis of the results obtained would be incomplete without assessing the spatial homogeneity of the crystal structure of the samples under study. To visualize the distribution of the amorphous and crystalline phases in laser-treated silicon coatings, two-dimensional maps of the sample surface were constructed based on the results of the RS measurements. Figure 2 shows a map for a sample processed at a fluence of 18.2 J/cm^2. Each map point in Fig. 2, *a* represents the integral RS intensity in the range from 500 to 525 cm^{-1} for the crystalline phase of silicon,

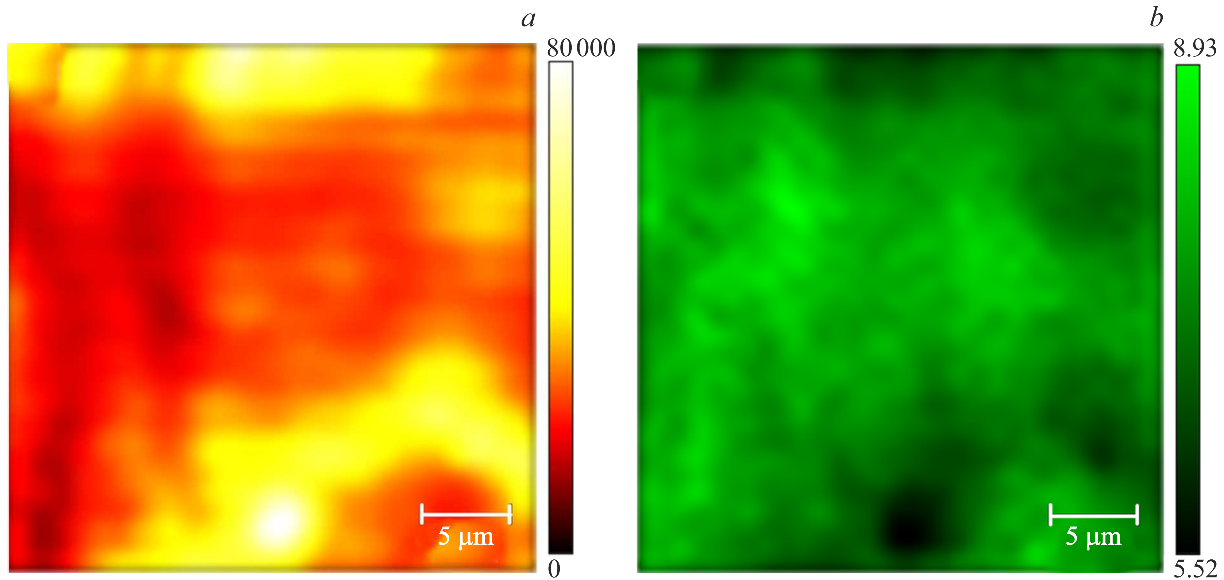

Figure 2. RS maps for the crystalline phase of silicon sample on a PI substrate: *a* — peak area, *b* — width at half maximum. The sample was processed at a fluence of 18.2 J/cm^2.

Table 2. Results of studies of samples on non-woven substrates using the RS method

Fluence, J/cm^2	Position of the peak,cm^{-1}	Width at half maximum, cm^{-1}	Integral intensity of the peak
0.457	519.8	5.52	25281.3
0.426	519.8	5.38	25056.81
0.4	519.88	5.94	22638.23
0.377	520.08	5.06	30911.18
0.364	519.94	5.81	17983.82
0.352	519.57	6.07	24182.07
0.341	519.64	6.41	19821.13
0.331	519.23	6.7	13924.57
0.32	519.51	6.57	18882.55
0.293	519.27	7.99	10778.78
0.285	519.1	6.92	9822.67
0.279	519.14	7.08	16417.18

and in Fig. 2, *b* half-width value for the peak of the TO mode of the crystalline phase.

Since the map in Fig. 2, *a* was generated for the range from 500 to 525 cm^{-1}, it illustrates the intensity of the TO mode of crystalline silicon and, accordingly, the bright areas correspond to the signal of the crystalline phase of silicon with the highest intensity. The figure shows that the signal at all points on the map is different from zero, i.e. the sample does not contain non-crystallized areas, which confirms the above results.

The map in Fig. 2, *b* actually copies the intensity map of the crystalline TO mode, but in inverted form. This result is quite logical, since the better the crystal structure of silicon is ordered at the point of analysis, the more intense and narrower the RS peak is due to better synchronization of phonon vibrations.

Figure 3, *a* shows the intensity map of the TO mode peak of the crystalline phase of silicon for a sample processed at a fluence of 8.42 J/cm^2. The homogeneity here is much worse; the crystalline phase is detected only at some points. The size of the crystallized areas is on the order of several micrometers. Figure 3, *b* shows a map of the integral RS intensity of the same sample in the range from 200 to 490 cm^{-1}. In this range, the signal intensity is mainly determined by the LO and TO modes of amorphous silicon. The amorphous phase is visualized in the form of fairly large areas with uniform RS signal intensity, and these areas include areas with a signal from the crystalline phase. However, there are areas in both maps in which there is no signal from either the amorphous or crystalline phases. Most likely, these areas are covered with residual aluminum, which shields the underlying silicon layer from the probing laser beam. Thus, at low laser processing fluences, aluminum ablates from the silicon surface only partially [23]. Moreover, even in areas with a removed aluminum layer, the formation of the crystalline phase occurs to a limited extent.

2.2. Samples on non-woven PAN

For samples on nonwoven PAN substrates, a larger number of modes were tested due to the fibrous structure

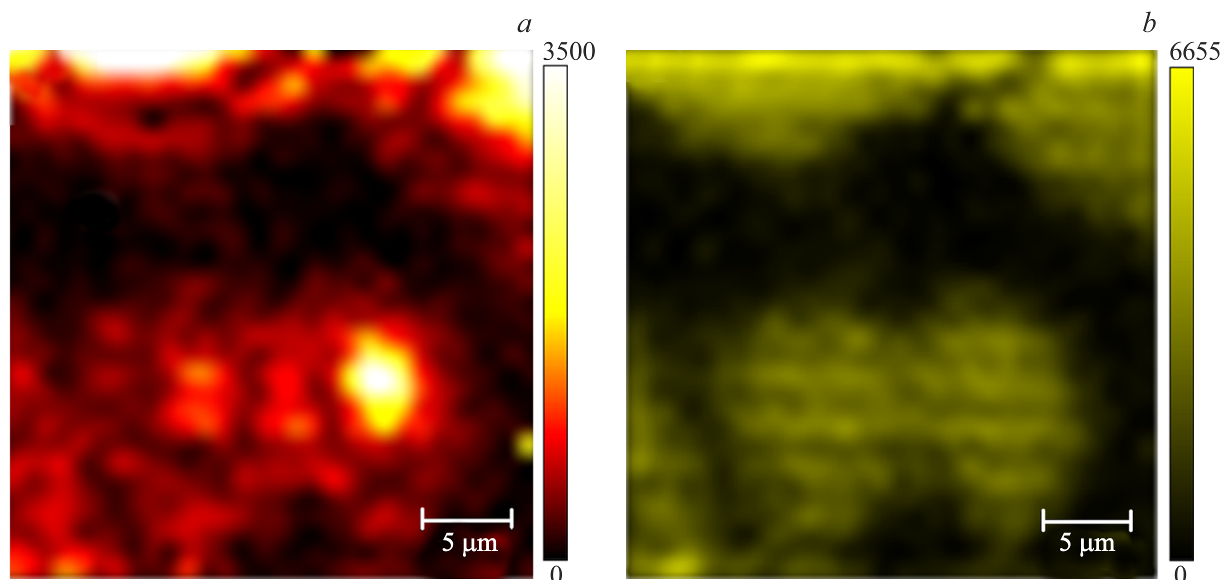

Figure 3. Peak area maps for a sample on a polyimide substrate (fluence 8.42 J/cm^2): *a* — in the range from 500 to 525 cm^{-1}, *b* — in range from 200 to 490 cm^{-1}.

of the substrate and the lack of information in the scientific literature on the mechanisms of laser radiation action on materials of this kind with coatings undergoing a phase transition.

The results of RS spectroscopy for the studied samples are given in Table 2.

It should be noted that the position of the peak of the TO mode of crystalline silicon for all modes exceeds 519 cm^{-1}, which is significantly closer to single crystal silicon than for samples on PI substrates. The half-width is also generally smaller than for thicker samples on PI films. This fact may indicate a more homogeneous crystallization of thin and spatially limited silicon coatings by polymer fibers than thick and macro-sized silicon coatings.

The results shown in Table 2 are further illustrated using Fig. 4.

The spectra also indicate the presence of crystallization, with no amorphous phase peaks detected for all three fluences. The integrated intensity of the peak decreases as the laser exposure decreases, and the width, on the contrary, increases. This suggests that as the fluence decreases, the quality of the crystalline structure of the silicon coating deteriorates. However, it is not possible to significantly increase the fluence. The glass transition temperature of PAN fibers obtained by electrospinning is 377 K [24]. If the specified temperature is reached or exceeded during annealing, then after its completion the fibers will lose their flexibility and become brittle, which will subsequently lead to their damage when the sample is bent.

The above consideration was confirmed using SEM. SEM images of the surface of the samples under study, illustrating the change in the state of the coating and substrate depending on the fluence of laser radiation, are shown in Fig. 5.

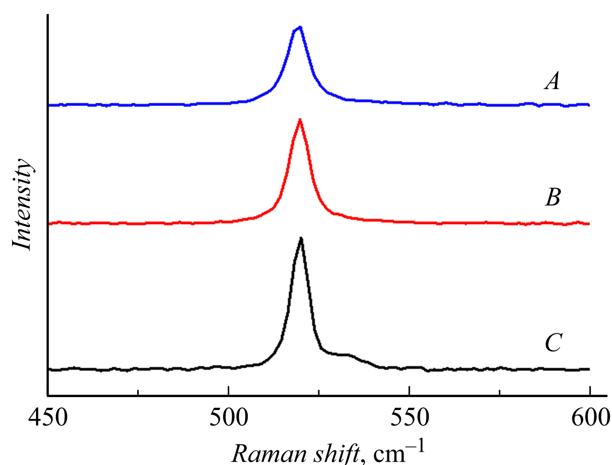

Figure 4. RS spectra of a sample on a non-woven substrate, where *A* — spectrum of a section of the sample processed with a fluence of 0.279 J/cm^2; *B* — spectrum of a sample area processed with a fluence of 0.341 J/cm^2; *C* — spectrum of a sample area processed with a fluence of 0.457 J/cm^2.

It can be seen from the figure that during laser processing, some of the fibers break or are completely destroyed, after which only empty half-shells remain, on the surface of which particles are formed, which go up with increasing fluence. The average diameters of fibers, half-shells and particles are given in Table 3.

Sputtered fibers that have not been subjected to laser annealing have the smallest average diameter (493 nm). The fibers in areas of the sample that were laser processed with high fluence values also have a relatively small diameter. As the fluence decreases, there is a tendency for the fiber diameter to increase, which can be explained by

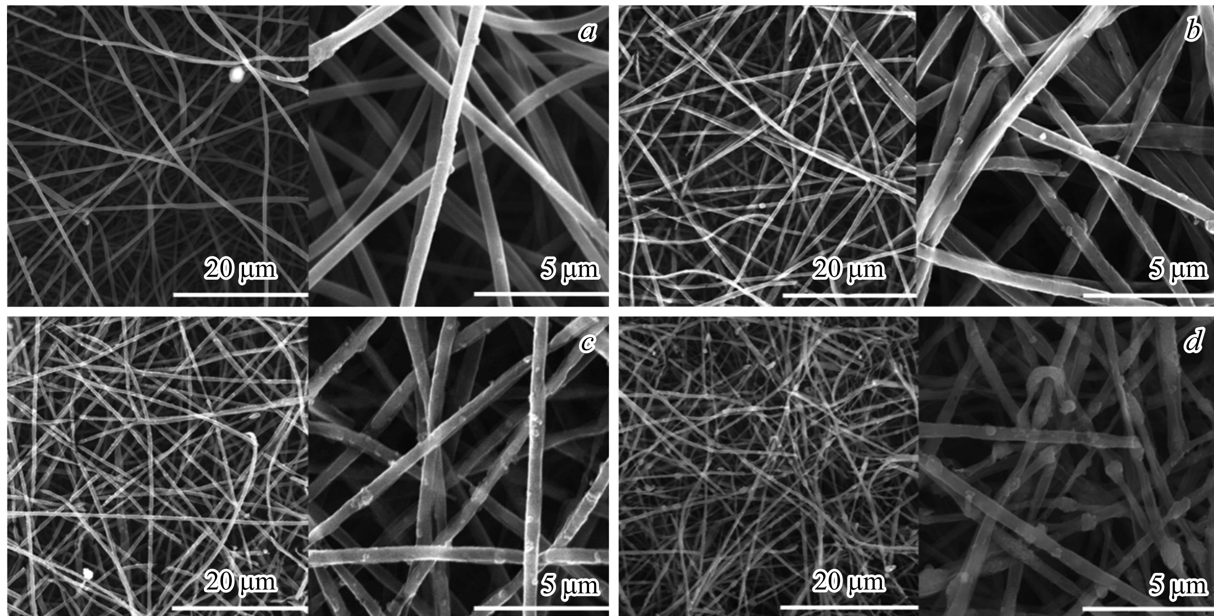

Figure 5. SEM images of various sections of the sample on a non-woven substrate with deposited layers of silicon and aluminum: *a* — section not treated with laser; *b* — area treated with a laser with a fluence of 0.279 J/cm^2; *c* — area treated with a laser with a fluence of 0.341 J/cm^2; *d* — area treated with a laser with a fluence of 0.457 J/cm^2.

Table 3. Results of studies of samples on non-woven substrates using SEM

Fluence, J/cm^2	Diameter, nm			Number of damaged threads, pcs.
	Fibers	Half-shells	Particles	
0.457	534	352	502	99
0.426	540	441	386	96
0.4	596	397	344	92
0.377	637	394	361	62
0.364	640	458	327	58
0.352	688	440	327	52
0.341	608	434	385	49
0.331	685	424	372	51
0.32	591	399	354	51
0.293	677	389	335	38
0.285	617	385	350	29
0.279	712	423	354	27

its thermal expansion [25]. The work [26] showed that as the temperature increases, the density of PAN fibers increases. This may explain the behavior of fibers during laser annealing. The temperature in the annealed spot depends on the fluence; the larger it is, the greater the heating. Accordingly, during laser processing, two competing processes occur: thermal expansion of the fibers and densification of their structure. As a result, at high fluences, the diameter of the fibers begins to tend to the original diameter of the fibers before laser treatment.

To assess the condition of the nonwoven substrate after laser annealing, the number of damaged fibers in SEM images was calculated. The results are also given in Table 3.

As can be seen from the table, when the fluence is reduced by only 0.04 J/cm^2, the number of damaged fibers

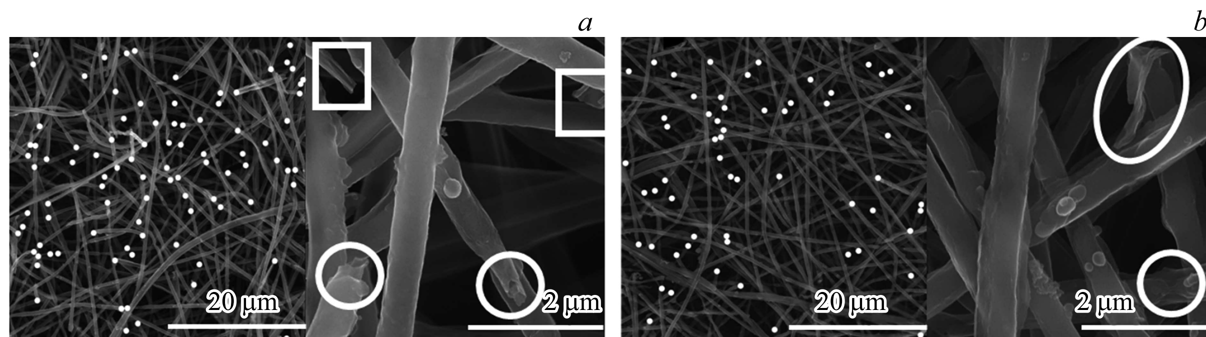

Figure 6. SEM images of a sample on a non-woven substrate with marked damaged threads: *a* — area treated with a laser with a fluence of 0.4 J/cm^2; *b* — area treated with a laser with a fluence of 0.36 J/cm^2. Damaged fibers are marked with ovals, areas with missing fibers are marked with squares.

noticeably decreases. Thus, at a fluence equal to 0.4 J/cm^2, 92 damaged fibers were recorded in the SEM image, and at a fluence equal to 0.364 J/cm^2, — 58 damaged fibers. In Fig. 6 the fibers damaged as a result of laser processing of the sample are marked in white. Meanwhile, it can be noted that on the sample processed at a fluence of 0.4 J/cm^2, there are empty half-shells (marked with squares). Thus, it can be assumed that when the limit value of the fluence (0.4 J/cm^2) is exceeded, destruction of the polymer fibers occurs.

When choosing the optimal laser processing mode, it should be taken into account that the number of damaged fibers should be minimal in order to maintain the integrity of the substrate. At the same time, laser processing modes with the lowest fluences cannot be considered as the most optimal, since, according to RS spectroscopy results, they are inferior to other modes in the crystallinity of the resulting silicon coating.

2.3. Proposed mechanism of crystallization

Taking into account the above results, we can assume the following mechanism of silicon crystallization. The work [27] showed that the appearance of D- and G-modes of carbon in the RS spectrum of polyimide is possible at a temperature of 833 K. In this case, on the sample processed at 18.2 J/cm ^{2}, no carbon peaks appeared in the RS spectrum, which indicates the absence of carbonization of the substrate, and crystallization of silicon occurred. On the other hand, it is known [28] that aluminum can reduce the temperature of formation of the crystalline phase to 623 K. Consequently, crystallization of silicon on PI substrates most likely occurs in the range 623–833 K, which is lower than the eutectic temperature for the Si–Al system (850 K). Thus, the most probable mechanism is solid-phase crystallization, described in a recent work [29]. The silicon layer turns out to be limited, on the one hand, by a „cold“ PI substrate, and on the other by a „“ hot aluminum layer that has absorbed the laser radiation energy. A sharp temperature gradient is formed in the silicon layer, which contributes to the formation of significant mechanical stresses, and interatomic bonds soften. This is followed by destabilization and disorder of the lattice, reminiscent of melting, although still on a cold lattice. In the process of stress relaxation, a reverse ordering process occurs, leading to a structure with minimal potential energy, i.e. crystalline. In this case, rapid cooling down of the silicon layer leads to the formation of many small nanocrystallites.

The aluminum layer not only absorbs laser radiation, but also provides a more uniform distribution of thermal energy over the silicon surface, which makes it possible to obtain a uniformly crystallized silicon layer (Fig. 2, *a*). Meanwhile, it cannot be ignored the opportunity of introducing aluminum into the silicon coating due to diffusion [30].

There is a similar situation in the case of crystallization on nonwoven PAN substrates. Here the limitation is further enhanced; the dimensions of the silicon coating are limited not only by thickness, but also by fiber diameter. As a result, crystallization is even more successful, although the values of the fluences required for this are an order of magnitude lower. In addition, there is an interesting phenomenon: submicron particles are formed on the fibers. These particles are probably formed from aluminum residues that have not undergone ablation. It can be assumed that these are frozen drops that moved along the fibers during laser processing. It is worth noting that the silicon coating remains continuous and without kinks.

Conclusion

During the study, samples of crystallized silicon coatings on flexible film and fibrous polymer substrates were obtained and studied. The conducted studies confirm the prospects of using the MILS crystallization technique for obtaining nanocrystalline silicon coatings on low-melting substrates.

For samples on PI film, completely crystallized silicon was obtained over an area $30 \times 30\,\mu$m. It is also worth noting that the thickness of the crystallized silicon layer was $1\,\mu$m. Such results allow us to talk about the prospects for

using MILS crystallization in the industrial production of microelectronic devices and solar cells.

In the case of nonwoven substrates based on PAN, we can talk about a certain range of laser radiation intensity, in which it is possible to achieve the optimal ratio of silicon crystallinity and substrate integrity. This range was $0.341-0.377\,J/cm^2$.

Based on the experimental results obtained, a mechanism for the formation of nanocrystalline silicon coatings has been proposed, which explains the formation of the crystalline phase at temperatures not exceeding the melting point of silicon and the formation of eutectic in the aluminum-silicon system.

Funding

The study was supported by a grant from the Russian Science Foundation № 23-22-00047, https://rscf.ru/project/23-22-00047/.

Conflict of interest

The authors declare that they have no conflict of interest

References

[1] M. Benelmekki, A. Erbe. Front. Nanosci, **14**, 1 (2019). DOI: 10.1016/B978-0-08-102572-7.00001-5
[2] H.Y. Xu, M.K. Akbari, S. Zhuiykov. Nanoscale Res. Lett., **16** (1), 94 (2021). DOI: 10.1186/s11671-021-03551-w
[3] R. Zhang. Appl. Comput. Eng., **23** (1), 96 (2023). DOI: 10.54254/2755-2721/23/20230618
[4] A.J. Lovett, V. Daramalla, D. Nayak, F. N. Sayed, A. Mahadevegowda, C. Ducati, B.F. Spencer, S.E. Dutton, C.P. Grey, J.L. MacManus-Driscoll. Adv. Energy Mater., **13** (38), 2302053 (2023). DOI: 10.1002/aenm.202302053
[5] T.M. Mazur, V.V. Prokopiv, M.P. Mazur, U.M. Pysklynets. Phys. Chem. Solid State, **22** (4), 817 (2021). DOI: 10.15330/pcss.22.4.817-827
[6] L. Feng, S. Song, H. Li, R. He, S. Chen, J. Wang, G. Zhao, X. Zhaol. Metals, **13** (4), 792 (2023). DOI: 10.3390/met13040792
[7] S. Sreejith, J. Ajayan, Sreedhar Kollem, B. Sivasankari. Silicon, **14**, 8277 (2022). DOI: 10.1007/s12633-021-01644-w
[8] J. Hou, B. Yang, X. Li, C. Ma, B. Wang, H. Long, Ch. Yang, Sh. Chen. J. Nanophoton., **14** (1), 016008 (2020). DOI: 10.1117/1.JNP.14.016008
[9] N. Vouroutzis, J. Stoemenos, N. Frangis, G.Z. Radnóczi, D. Knez, F. Hofer, B. Pécz. Sci. Rep., **9**, 1, (2019). DOI: 10.1038/s41598-019-39503-9
[10] M.D. Efremov, V.A. Volodin, L.I. Fedina, A.A. Gutakovsky, D.V. Marin, S.A. Kochubey, A.A. Popov, Yu.A. Minakov, V.N. Ulasyuk. Pisma v ZhTF, **29** (13), 89 (2003) (in Russian).
[11] T.T. Korchagina, V.A. Volodin, A.A. Popov, K.S. Khorkov, M.N. Gerke. Tech. Phys. Lett., **37** (7), 622 (2011). DOI: 10.1134/S1063785011070091
[12] A.A. Serdobintsev, I.O. Kozhevnikov, A.V. Starodubov, P.V. Ryabukho, V.V. Galushka, A.M. Pavlov. Phys. Status Solidi A, **216** (11) 1800964 (2019). DOI: 10.1002/pssa.201800964
[13] A.A. Serdobintsev, V.A. Luzanov, I.O. Kozhevnikov, P.V. Ryabukho, D.M. Mitin, D.N. Bratashov, A.V. Starodubov, A.M. Pavlov. J. Phys. Conf. Ser., **1400**, 1, (2019). DOI: 10.1088/1742-6596/1400/5/055034
[14] F.A. Samokhvalov, N.I. Smirnov, A.A. Rodionov, A.O. Zamchiy, E.A. Baranov, Yu.G. Shukhov, A.S. Fedotov, S.V. Starinskiy. Thermophys. Aeromechan., **30** (2), 361 (2023). DOI: 10.1134/S0869864323020178
[15] L.D. Volkovoynova, I.O. Kozhevnikov, A.M. Pavlov, A.A. Serdobintsev, A.V. Starodubov. Proceed. 8th Intern. Congress on Energy Fluxes and Radiation Effects (EFRE-2022), **8**, 916 (2022). DOI: 10.56761/EFRE2022.C3-P-005701
[16] V.A. Terekhov, E.I. Terukov, Yu.K. Undalov, K.A. Barkov, N.A. Kurilo, S.A. Ivkov, D.N. Nesterov, P.V. Seredin, D.L. Goloshchapov, D.A. Minakov, E.V. Popova, A.N. Lukin, I.N. Trapeznikova. Symmetry, **15** (9), 1800 (2023). DOI: 10.3390/sym15091800
[17] K. Shrestha. Mater. Res. Society, **1757**, 6 (2014). DOI: 10.1557/opl.2014.962
[18] K. Fabisiak, K. Wielki, W. Franków, P. Popielarski, A. Dychalska. Walter de Gruyter GmbH, **33**, 7 (2015). DOI: 10.1515/msp-2015-0067
[19] F. Raimondi, S. Abolhassani, R. Brütsch, F. Geiger, T. Lippert, J. Wambach, J. Wei, A. Wokaun. J. Appl. Phys., **88** (6), 3659 (2000). DOI: 10.1063/1.1289516
[20] D.M. Zhigunov, G.N. Kamaev, P.K. Kashkarov, V.A. Volodin. Appl. Phys. Lett., **113**, 5 (2018). DOI: 10.1063/1.5037008
[21] J. Zi, H. Büscher, C. Falter, W. Ludwig, K. Zhang. Appl. Phys. Lett., **69**, 200 (1996). DOI: 10.1063/1.117371
[22] V.A. Volodin, V.A. Sachkov. J. Experiment. Theor. Phys., **116** (1), 100 (2013). DOI: 10.1134/S1063776112130183
[23] L.D. Volkovoinova, A.A. Serdobintsev. FTT **12**, 2177 (2023) (in Russian). DOI: 10.61011/FTT.2023.12.56753.5004k
[24] W.S. Khan, M. Ceylan, A. Jabarrania, L. Saeednia, R. Asmatulu. J. Thermal Eng., **3** (4), 1375 (2017). DOI: 10.18186/JOURNAL-OF-THERMAL-ENGINEERING.330180
[25] B.M. Tarakanov, O.A. Andreeva. Vysokomolekulyarnye soedineniya, **A32** (10), 2105 (1990) (in Russian).
[26] L. Chen, Zh. Shen, J. Liu, J. Liang, X. Wang. RSC Adv., **10** (11), 6356 (2020). DOI: 10.1039/C9RA08881D
[27] T. Kato, Y. Yamada, Y. Nishikawa, H. Ishikawa, S. Sato. Carbon, **178**, 58 (2021). DOI: 10.1016/j.carbon.2021.02.090
[28] G.J. Qi, S. Zhang, T.T. Tang, J.F. Li, X.W. Sun, X.T. Zeng. Surf. Coat. Technol., **198** (1–3), 300 (2005). DOI: 10.1016/j.surfcoat.2004.10.092
[29] I. Mirza, A.V. Bulgakov, H. Sopha, S.V. Starinckiy. Frontiers in Nanotechnol., **5**, 1 (2023). DOI: 10.3389/fnano.2023.1271832
[30] S.O. Solodovnikova, L.D. Volkovoynova, A.A. Serdobintsev, A.V. Starodubov, I.O. Kozhevnikov, A.M. Pavlov. J. Phys.: Conf. Series, **2103**, 012123 (2021). DOI: 10.1088/1742-6596/2103/1/012123

Translated by A.Akhtyamov